Discontinuous Galerkin Time Domain Method for Scattering Analysis of Air-Inlets

S. Gao [1], M. Liu [2], and Q. Cao [1]

[1] College of Electronic and Information Engineering
Nanjing University of Aeronautics and Astronautics, Nanjing, 210016, People's Republic of China
gaosiping@gmail.com, qunsheng@gmail.com

[2] Shanghai Institute of Satellite Engineering
Shanghai, 200240, People's Republic of China
liumeilin.cn@gmail.com

Abstract ─ In this paper, a high-order three dimensional (3-D) discontinuous Galerkin time domain (DGTD) method has been introduced for the first time for the efficient scattering analysis of air-inlets. This method combines the geometrical versatility of finite element method (FEM) with the explicit time-stepping of finite volume time domain (FVTD) method, thus having the advantages of handling electrically large, arbitrarily shaped, and complex media objects. To validate the capability of this method, the radar cross section (RCS) of three typical air-inlet models have been simulated. The results of the DGTD method agree well with that of the method of moments (MoM), which proves the DGTD method a useful alternative to the traditional methods to solve the scattering problems.

Index Terms ─ Air-inlets, DGTD, and RCS.

I. INTRODUCTION

Scattering properties of air-inlets is of great importance in radar signature analysis [1], as the air-inlets could significantly affect the overall RCS from jetfighters. Therefore, the development of accurate and efficient methods to evaluate the RCS from such structures is an important task and has attracted much attention in the computational electromagnetics community.

Classic frequency methods of scattering analysis include high frequency methods and low frequency methods. However, the high frequency methods employing ray tracing techniques [2] are less accurate when dealing with cavity structures, while the low frequency methods like the MoM [3] is hard to deal with electrically large and complex objects with dielectric coating. Moreover, as the increasing needs for the wideband scattering information, time domain method is more efficient, nonetheless, classic time domain methods such as the finite difference time domain (FDTD) method [4] and the finite element method time domain (FEMTD) [5] suffer from low accuracy or great resource consumption. As a result, new time domain method for efficiently solving the electrically large and complex scattering problem is highly desirable.

Recently a set of high-order DGTD methods has been developed [6-9], which commonly combines the geometrical versatility of the FEM [5] and the explicit time-stepping of the FVTD method [10]. It exceeds FDTD and FEMTD in accuracy and efficiency respectively [11], thus becoming a very suitable method for the electrically large, arbitrarily shaped, and complex media targets. Therefore, in this paper, for the first time, the high-order 3-D DGTD method is applied for the RCS evaluation of air-inlets. To validate the capability of this method to solving scattering problem, three typical air-inlet models have been simulated. The results of them have shown good agreement with that of the MoM, which proves the DGTD method a useful alternative to the other numerical methods.

Submitted On: Oct. 8, 2012
Accepted On: Apr. 16, 2013

The remaining parts of the paper are organized as follows. In section II, the DGTD method is briefly presented. In section III, several numerical results of air-inlet models are given to verify the accuracy of the method. Finally, conclusions are drawn in section IV.

II. DGTD FUNDAMENTALS

To introduce the high-order 3D DGTD method simply, the Maxwell's curl equations in linear, isotropic, and homogeneous media are presented in conservation form first,

$$\boldsymbol{\mathcal{Q}} \cdot \partial_t \boldsymbol{q} + \nabla \cdot \boldsymbol{F}(\boldsymbol{q}) = 0, \tag{1}$$

where the material matrix $\boldsymbol{\mathcal{Q}}$, the state vector $\boldsymbol{q}$, and the flux $\boldsymbol{F}$ are denoted as follows,

$$\boldsymbol{\mathcal{Q}} = \begin{bmatrix} \varepsilon & \\ & \mu \end{bmatrix}, \qquad \boldsymbol{q} = \begin{bmatrix} \boldsymbol{E} \\ \boldsymbol{H} \end{bmatrix},$$

$$\boldsymbol{F}_i(\boldsymbol{q}) = \begin{bmatrix} -\hat{\boldsymbol{e}}_i \times \boldsymbol{H} \\ \hat{\boldsymbol{e}}_i \times \boldsymbol{E} \end{bmatrix}, \; i = x, y, z.$$

Then, considering a 3D physical domain Ω, which is discretized by K non-overlapping elements (tetrahedrons in 3D), Ω^k, k=1…K. In an arbitrary element Ω^k, the fields can be expanded using Lagrange interpolation polynomials $L_i(\boldsymbol{r})$

$$\boldsymbol{q}^k(\boldsymbol{r}, t) \approx \sum_{i=1}^{N_p} \hat{\boldsymbol{q}}_i^k(t) L_i(\boldsymbol{r}), \tag{2}$$

where N_p represents the number of the local expansion. $\hat{\boldsymbol{q}}^k$ contains a N_p-vector of expansion coefficients to be solved. The relationship between N_p and the polynomial expansion order N for tetrahedron is N_p = (N+1)(N+2)(N+3)/6. A carefully chosen set of the interpolation nodes $\boldsymbol{r}_i$ could lead to good numerical behaviour [12].

Next, using the classic Galerkin method, equation (1) is sampled with test function $L_i(\boldsymbol{r})$ as shown,

$$\int_{\Omega^k} \left(\boldsymbol{\mathcal{Q}}^k \cdot \partial_t \hat{\boldsymbol{q}}^k + \nabla \cdot \boldsymbol{F}(\hat{\boldsymbol{q}}^k) \right) \cdot L_i(\boldsymbol{r}) d\boldsymbol{r} = 0. \tag{3}$$

In order to couple with the neighbouring elements, the divergence part of the integral in equation (3) is first manipulated by an integration by parts as

$$\int_{\Omega^k} \left(\boldsymbol{\mathcal{Q}}^k \cdot \partial_t \hat{\boldsymbol{q}}^k \cdot L_i(\boldsymbol{r}) - \boldsymbol{F}(\hat{\boldsymbol{q}}^k) \cdot \nabla L_i(\boldsymbol{r}) \right) d\boldsymbol{r} = - \int_{\partial\Omega^k} \left(\hat{\boldsymbol{n}}^k \cdot \boldsymbol{F}(\hat{\boldsymbol{q}}^k) \right) \cdot L_i(\boldsymbol{r}) d\boldsymbol{r},$$

where $\hat{\boldsymbol{n}}^k$ denotes the unit outward-pointing vector normal to the contour of element Ω^k denoted by $\partial\Omega^k$. Then, replace the flux $\boldsymbol{F}$ on the RHS by the numerical flux $\boldsymbol{F}^*$ and perform another integration by parts, the strong variational formulation of equation (3) can be obtained as,

$$\int_{\Omega^k} \left(\boldsymbol{\mathcal{Q}}^k \cdot \partial_t \hat{\boldsymbol{q}}^k + \nabla \cdot \boldsymbol{F}(\hat{\boldsymbol{q}}^k) \right) \cdot L_i(\boldsymbol{r}) d\boldsymbol{r} = \int_{\partial\Omega^k} \hat{\boldsymbol{n}}^k \cdot \left(\boldsymbol{F}(\hat{\boldsymbol{q}}^k) - \boldsymbol{F}^*(\hat{\boldsymbol{q}}^k) \right) \cdot L_i(\boldsymbol{r}) d\boldsymbol{r}. \tag{4}$$

The numerical flux $\boldsymbol{F}^*$ on the surface $\partial\Omega^k$ is to exchange the coupling between neighboring elements. It can be obtained properly by solving a local Riemann problem [6]. Here, the pure upwind flux [13] is used, which could strongly damp the unphysical modes [6],

$$\hat{\boldsymbol{n}} \cdot \left(\boldsymbol{F}(\hat{\boldsymbol{q}}^k) - \boldsymbol{F}^*(\hat{\boldsymbol{q}}^k) \right) = \begin{bmatrix} -\bar{Z}^{-1} \hat{\boldsymbol{n}} \times (Z^+ [\boldsymbol{H}^k] - \hat{\boldsymbol{n}} \times [\boldsymbol{E}^k]) \\ \bar{Y}^{-1} \hat{\boldsymbol{n}} \times (Y^+ [\boldsymbol{E}^k] + \hat{\boldsymbol{n}} \times [\boldsymbol{H}^k]) \end{bmatrix}, \tag{5}$$

where $[\boldsymbol{E}] = \boldsymbol{E}^- - \boldsymbol{E}^+$ and $[\boldsymbol{H}] = \boldsymbol{H}^- - \boldsymbol{H}^+$ measure the jump in the field values across element interfaces; i.e., superscript "+" refers to field values from the neighbor element while the "–" refers to field values local to the element. For the possible difference of material properties between two elements, local impedance and conductance, $Z^\pm = (Y^\pm)^{-1} = \sqrt{\mu^\pm / \varepsilon^\pm}$ and local sums $\bar{Z} = Z^+ + Z^-$, $\bar{Y} = Y^+ + Y^-$ has to be defined.

Finally, by substituting the expansions in equation (2) with the numerical flux of equation (5) into equation (4) and assuming parameters ε and μ constant in each element, the explicit expressions of the DGTD can be easily obtain as follows,

$$\begin{aligned} \frac{\partial \boldsymbol{E}^k}{\partial t} &= \frac{(\boldsymbol{\mathcal{M}}^k)^{-1}}{\varepsilon^k} \left(\boldsymbol{\mathcal{S}}^k \times \boldsymbol{H}^k - \boldsymbol{\mathcal{F}}^k \frac{\hat{\boldsymbol{n}} \times (Z^+ [\boldsymbol{H}^k] - \hat{\boldsymbol{n}} \times [\boldsymbol{E}^k])}{\bar{Z}} \right), \\ \frac{\partial \boldsymbol{H}^k}{\partial t} &= \frac{(\boldsymbol{\mathcal{M}}^k)^{-1}}{\mu^k} \left(-\boldsymbol{\mathcal{S}}^k \times \boldsymbol{E}^k + \boldsymbol{\mathcal{F}}^k \frac{\hat{\boldsymbol{n}} \times (Y^+ [\boldsymbol{E}^k] + \hat{\boldsymbol{n}} \times [\boldsymbol{H}^k])}{\bar{Y}} \right). \end{aligned} \tag{6}$$

Here, $\boldsymbol{E}^k$ and $\boldsymbol{H}^k$ are N_p-vectors. The mass matrix $\boldsymbol{\mathcal{M}}^k$, the stiffness matrices $\boldsymbol{\mathcal{S}}^k$, and the face mass matrix $\boldsymbol{\mathcal{F}}^k$ with respect to the element contour $\partial\Omega$k are defined as shown below

$$\begin{aligned} (\boldsymbol{\mathcal{M}}^k)_{ij} &= \int_{\Omega^k} L_i(\boldsymbol{r}) L_j(\boldsymbol{r}) d\boldsymbol{r}, \\ (\boldsymbol{\mathcal{S}}_m^k)_{ij} &= \int_{\Omega^k} L_i(\boldsymbol{r}) \partial_m L_j(\boldsymbol{r}) d\boldsymbol{r}, \; m \in \{x, y, z\}, \\ (\boldsymbol{\mathcal{F}}^k)_{ij} &= \int_{\partial\Omega^k} L_i(\boldsymbol{r}) L_j(\boldsymbol{r}) d\boldsymbol{r}, \quad j \in \left\{ j \mid \boldsymbol{r}_j \in \partial\Omega^k \right\}. \end{aligned}$$

Since equation (6) are ordinary differential

equations with respect to time, a 4th-order, five-stage, low-storage Runge-Kutta scheme [14] is employed for the time integration.

III. NUMERICAL RESULTS

In this section, we present several numerical results to validate the accuracy of the DGTD method while solving the scattering problem of air-inlets. The 3rd-order Lagrange polynomial is employed as the basis function. And a commercial MoM is employed for comparison. Figure 1 shows the computational setup of the air-inlet model. For simplicity here, the electrically large air-inlet is considered as a long perfect electric conducting cylindrical waveguide with a closed-end (deep cavity). It is placed in the center of the total field (TF). A two-cell perfectly matched layer (not depicted here) is wrapped around the scattering field (SF) in order to truncate the computational area. A modulation Gaussian pulse (φ =180°, θ = 0°, polarization angle = 0°) is injected using the TF/SF technique [4].

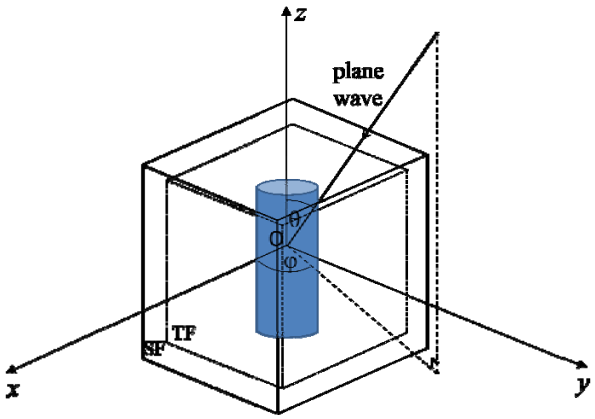

Fig. 1. Computational setup of the air-inlet model.

Figures 2 to 4 show three numerical results and their corresponding model insets. The models are the straight, the frustum, and the bending air-inlet models as shown in Figs. 2b to 4b, respectively. Each model is 10λ length and 0.5λ radius, except that the radius of frustum one varies from 0.5λ to 0.25λ, and the bending one bends 90° from the z-direction at the rear. They are all meshed with tetrahedrons of 0.1λ edge-length.

Two comparable bistatic RCS results at 300 MHz are shown in Figs. 2a to 4a, which are the blue circle curves by the DGTD method and the red line curves by the MoM using FEKO v6.1. All the RCS values are evaluated at the direction of φ = 0°, θ from 0° to 360° with 1° increment. From these values, although the air-inlets models are various and electrically long, we could observe great agreement between the results of these two methods. Among these values, the majors mainly appear at the front (θ = 0°) and back (θ = 180°) of the air-inlet models. It could be caused by the direction of the incident plane wave and its multiple reflections by the deep cavity.

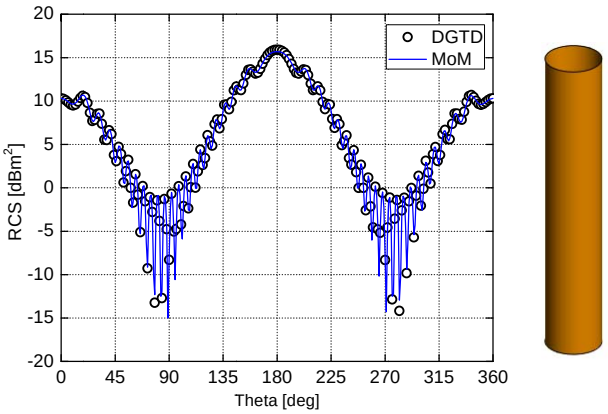

(a) (b)

Fig. 2. (a) the bistatic RCS results and (b) the inset of the straight air-inlet model.

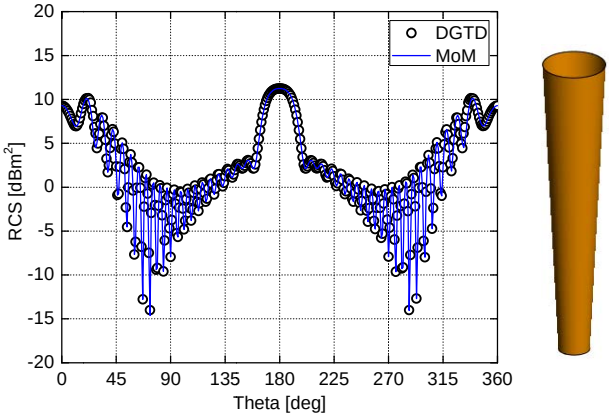

(a) (b)

Fig. 3. (a) the bistatic RCS results and (b) the inset of the frustum air-inlet model.

The time consumed by the numerical examples using the DGTD method is a bit longer than the commercial MoM under the same circumstance, which is the platform of the ThinkPad T420 with the Intel® Core™ i7-2640M CPU with 2.80 GHz (only one core is used) and 4.0 GB RAM. However, considering the MoM is a

frequency domain method and the models in FEKO are meshed with 0.1λ edge-length on surface, the DGTD method would be a potential tool when dealing with wideband scattering problems of electrically larger and complex media air-inlet.

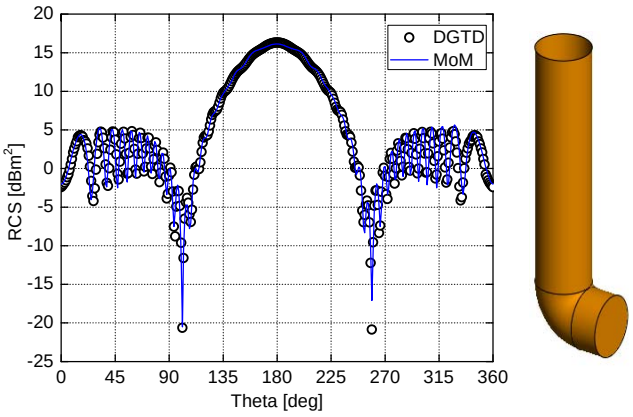

(a) (b)

Fig. 4. (a) the bistatic RCS results and (b) the inset of the bending air-inlet model.

IV. CONCLUSION

In this article, the high-order 3-D DGTD method has been introduced for the first time for the scattering analysis of air-inlets. This method has the advantages of handling electrically large, arbitrarily shaped, and complex media composition objects. The results of DGTD agree well with those of the MoM, which proves it to be a useful alternative to the traditional methods to solve the scattering problem. Considering the advantages of this method, it may be a promising method for electrically large and complex air-inlet in future work.

ACKNOWLEDGMENT

This work was supported by the project of the Priority Academic Program Development (PAPD) of Jiangsu Higher Education Institutions, and the China Scholarship Council (CSC).

REFERENCES

[1] J. Jin, "Electromagnetic scattering from large, deep, and arbitrarily-shaped open cavities," *Electromagnetics,* vol. 18, pp. 3-34, 1997.

[2] H. Ling, S.-W. Lee, and R.-C. Chou, "High-frequency RCS of open cavities with rectangular and circular cross sections," *IEEE Transactions on Antennas and Propagation,* vol. 5, pp. 648-654, 1992.

[3] C. C. Lu and C. Luo, "Comparison of iteration convergences of SIE and VSIE for solving electromagnetic scattering problems for coated objects," *Radio Science,* vol. 38, pp. 11/1-11/9, 2003.

[4] A. Taflove and S. C. Hagness, *Computational Electrodynamics: The Finite-Difference Time-Domain Method*: Artech House, 2005.

[5] J. M. Jin, *The Finite Element Method in Electromagnetics*: Wiley, 2002.

[6] J. S. Hesthaven and T. Warburton, *Nodal Discontinuous Galerkin Methods: Algorithms, Analysis, and Applications*: Springer, 2008.

[7] N. Canouet, L. Fezoui, and S. Piperno, "Discontinuous Galerkin time-domain solution of Maxwell's equations on locally-refined nonconforming Cartesian grids," *COMPEL - The International Journal for Computation and Mathematics in Electrical and Electronic Engineering,* vol. 24, pp. 1381-1401, 2005.

[8] E. Gjonaj and T. Weiland, "A projection penalization approach for the high-order DG-FEM in the time domain," *Radio Science,* vol. 46, 2011.

[9] S. D. Gedney, C. Luo, J. A. Roden, R. D. Crawford, B. Guernsey, J. A. Miller, T. Kramer, and E. W. Lucas, "The discontinuous Galerkin finite-element time-domain method solution of Maxwell's equations," *Applied Computational Electromagnetics Society Journal,* vol. 24, pp. 129-142, 2009.

[10] R. J. LeVeque, *Finite Volume Methods for Hyperbolic Problems*: Cambridge University Press, 2002.

[11] J. Alvarez, S. G. Garcia, L. D. Angulo, and A. R. Bretones, "Computational electromagnetic tools for EMC in aerospace," Marrakesh, 2011, pp. 1840-1844.

[12] T. Warburton, "An explicit construction of interpolation nodes on the simplex," *Journal of Engineering Mathematics,* vol. 56, pp. 247-262, 2006.

[13] J. S. Hesthaven and T. Warburton, "Nodal high-order methods on unstructured grids. I. Time-domain solution of Maxwell's equations," *Journal of Computational Physics,* vol. 181, pp. 186-221, 2002.

[14] M. H. Carpenter and C. A. Kennedy, "Fourth-order 2N-storage Runge-Kutta schemes," NASA Technical Memorandum 109112, 1994.